Nucleon-χ_{cJ} Dissociation Cross Sections

2002 Chinese Phys. Lett. 19 1602

(http://iopscience.iop.org/0256-307X/19/11/311)

Nucleon-χ_{cJ} Dissociation Cross Sections *

FENG You-Ceng(冯又层)[1], XU Xiao-Ming(许晓明)[2], ZHOU Dai-Cui(周代翠)[1]
Institute of Particle Physics, Central China Normal University, Wuhan 430079
Shanghai Institute of Nuclear Research, Chinese Academy of Sciences, PO Box 800204, Shanghai 201800

(Received 25 April 2002)

Nucleon-χ_{cJ} dissociation cross sections are calculated in a constituent interexchange model in which quark–quark potential is derived from the Buchmüller–Tye quark–anti-quark potential. These new cross sections for dominant reaction channels depend on the centre-of-mass energy of the nucleon and the charmonium.

PACS: 25.60.Dz, 14.40.Lb, 14.20.Lq

Interaction with hadronic secondaries and incoherent partonic effects, as well as all other effects considered so far, cannot produce a discontinuity in the J/ψ survival probability, unless one assumes that something dramatically occurs to J/ψ only after the "critical density" is achieved.[1] Several authors have assumed that, once the density of produced particles exceeds some critical value, the formation of a "deconfined phase"[2] takes place.

Relativistic heavy ion collision with a high-energy accelerator can provide the environment of high density and high temperature which leads to the occurrence of deconfinement. The run of ^{197}Au + ^{197}Au collisions at $\sqrt{S_{NN}} = 200\,$GeV at relativistic high ion collision (RHIC) has been realized. The new measurement of J/ψ at RHIC has become available and this has attracted great attention in the study of J/ψ production and suppression with different theoretical models. The direct J/ψ production has been studied in Ref. [3]. Since the prompt J/ψ production is to be measured, contributions from the radiative feedown of χ_{cJ} and the decay of ψ' must be included in the theoretical description. For example, the discontinuity of the $J/\psi/DY$ ratio in Pb–Pb collisions[4] appears as a result of dissociation of χ states at the deconfinement point; $\chi's$ contribute $\simeq 40\%$ to the J/ψ production.[5] The HERA-B collaboration has been measuring the χ_{cJ} suppression at DESY in proton–nucleus collisions. Their measured values at large negative x_F may give an insight into χ_{cJ} dissociation cross sections. Our cross sections calculated in this work are most relevant to their measurements and are used to interpret their results.[6]

Nucleus–nucleus collisons at RHIC and large hadron collision (LHC) energies have been divided into four stages:[7,8] initial parton–parton scatterings, prethermal gluon gas, thermalized parton plasma, and hadronic matter. Parton–parton scatterings in the four stages yield $c\bar{c}$ pairs, leading to the formation of physical resonances. Short-distance parton–parton reactions produce J/ψ pairs in colour octet or singlet states with a very small spatial distribution. Such a point-like $c\bar{c}$ has a certain probability to transit into the states of J/ψ, ψ' and χ_{cJ}. These processes are described in the nonrelativistic quantum chromodynamics (NRQCD).[9] The direct J/ψ production from the partonic system before the formation of hadronic matter has been presented in Ref. [3] in combination with $c\bar{c}$ in the prethermal and thermal stages. The cross section of $c\bar{c}$ dissociations due to gluons in the hot partonic system and mesons in hadronic matter has been discussed in Ref. [10].

In this Letter, we use the constituent interexchange method to calculate the charmonium dissociation cross section by baryons in the pseudoscalar octet and vector decuplet, which are calculated with a QCD-based potential developed from the Buchmüller–Tye potential. Then we can see the dependence of the cross section on the centre-of-mass energy of χ_{cJ} and the baryon. The magnitude comparison of $c\bar{c}$ dissociations due to partonic system, mesons in hadronic matter, baryons in hadronic matter are also presented.

While the production of charmonium can be understood within perturbative QCD due to the large mass of the charmed quark, its further interaction within surrounding matter is essentially soft in nature and cannot be treated perturbatively. It is of interest to calculate the dissociation cross section in the framework of an essentially nonperturbative approach based on a hadronic model that incorporates quark confinement.[11] Effective approaches to charmonium dissociation in the nonperturbative domain of strongly correlated quark matter consider this process as a quark-exchange (string-flip) process.[12] The quark-exchange processes of χ_{cJ} and the baryon ($c\bar{c} + q_1q_2q_3 \rightarrow q_1q_2c + q_3\bar{c}$) are divided into six diagrams according to the colour interactions via one gluon propagation between (1) q_1 and $\bar{c}$, (2) q_2 and $\bar{c}$, (3) q_3 and $\bar{c}$, (4) q_1 and c, (5) q_2 and c, (6) q_3 and c. Therefore the relativistic invariant matrix element is

$$\mathcal{M} = \mathcal{N}\langle \Psi_{q_1q_2q_3}|\langle \Psi_{c\bar{c}}|(V_{q_1\bar{c}} + V_{q_2\bar{c}} + V_{q_3\bar{c}}$$

* Supported by the National Natural Science Foundation of China under Grant No 10075022.

$$+ V_{q_1c} + V_{q_2c} + V_{q_3c})|\Psi_{q_1q_2c}\rangle|\Psi_{q_3\bar{c}}\rangle, \quad (1)$$

where $\mathcal{N} = 4\sqrt{E_{q_1q_2q_3}E_{c\bar{c}}E_{q_3\bar{c}}E_{q_1q_2c}}$, V_{ij} ($i = q_1, q_2, q_3$; $j = c, \bar{c}$) is the interaction potential between quark i and quark j. Ψ is the inner wavefunction of the meson and the baryon, which includes the space wavefunction, colour wavefunction, spin and flavour wavefunction.

The differential cross section of two-to-two process $(A(p_1) + B(p_2) \rightarrow C(p_3) + D(p_4))$ is given by

$$\mathrm{d}\sigma = \frac{|\mathcal{M}|^2}{64\pi^2 s}\frac{|\boldsymbol{p}'_{\mathrm{cm}}|}{|\boldsymbol{p}_{\mathrm{cm}}|}\mathrm{d}\Omega_{\mathrm{cm}}. \quad (2)$$

In the centre-of-mass frame of A and B, $\boldsymbol{p}_1 = -\boldsymbol{p}_2 = \boldsymbol{p}_{\mathrm{cm}}$, $\boldsymbol{p}_3 = -\boldsymbol{p}_4 = \boldsymbol{p}'_{\mathrm{cm}}$, $E_1 + E_2 = E_3 + E_4$, $(p_1+p_2)^2 = (p_3+p_4)^2 = s$. The total cross section of the two-to-two process is obtained by integrating over $z = \cos\theta(\boldsymbol{p}, \boldsymbol{p}')$:

$$\sigma = \frac{1}{32\pi s}\frac{|\boldsymbol{p}'_{\mathrm{cm}}|}{|\boldsymbol{p}_{\mathrm{cm}}|}\int_{-1}^{1}\mathrm{d}z|\mathcal{M}(\boldsymbol{p}_{\mathrm{cm}}, \boldsymbol{p}'_{\mathrm{cm}}, z)|^2, \quad (3)$$

where $\theta(\boldsymbol{p}, \boldsymbol{p}')$ is the angle between the relative momenta $\boldsymbol{p}$ and $\boldsymbol{p}'$ of incoming and outgoing particles, respectively. The core of formula (3) is the calculation of the relativistic invariant matrix element $\mathcal{M}$. The decision of $\mathcal{M}$ is due to the action potential and wavefunction.

The Buchmüller–Tye potential[13] is adopted here. It is cast from the relativistic potential which depends on the coordinate $\boldsymbol{r}$ of particles a and b

$$V_{ab}(\boldsymbol{r}) = -\frac{\boldsymbol{\lambda}_a}{2}\frac{\boldsymbol{\lambda}_b}{2}\frac{3}{4}Kr - \frac{\boldsymbol{\lambda}_a}{2}\frac{\boldsymbol{\lambda}_b}{2}16\pi^2 \cdot \int\frac{\mathrm{d}^3\boldsymbol{Q}}{(2\pi)^3}\frac{\rho(\boldsymbol{Q}^2) - K/\boldsymbol{Q}^2}{\boldsymbol{Q}^2}\gamma_0^a\gamma_\mu^a\gamma^{0b}\gamma^{\mu b}\mathrm{e}^{\mathrm{i}\boldsymbol{Q}\cdot\boldsymbol{r}}, \quad (4)$$

where $\rho(\boldsymbol{Q}^2)$ is a physical running coupling constant, $\gamma^\mu (\mu = 0, 1, 2, 3)$, $\boldsymbol{\alpha}$ are the Dirac matrices, $\boldsymbol{\lambda}$ are the Gell–Mann matrices, $\boldsymbol{Q}$ is the gluon momentum, and the string tension

$$K = \frac{1}{16\pi^2\alpha'}$$

with the Regge slope

$$\alpha' = 1.04\,\mathrm{GeV}^{-2}.$$

After carrying out the integration over $\boldsymbol{Q}$, Eq. (4) becomes

$$V_{ab}(\boldsymbol{r}) = V_{\mathrm{coul}}(\boldsymbol{r}) + V_{\mathrm{conf}}(\boldsymbol{r}) + V_{\mathrm{loop}}(\boldsymbol{r}) \quad (5)$$

where the three terms are

$$V_{\mathrm{coul}}(\boldsymbol{r}) = \frac{\boldsymbol{\lambda}_a}{2}\frac{\boldsymbol{\lambda}_b}{2}\left(\frac{6\pi}{2\pi r} - \frac{3\pi}{25}\frac{\boldsymbol{\alpha}^a\cdot\boldsymbol{\alpha}^b}{r} - \frac{3\pi}{25}\frac{\boldsymbol{\alpha}^a\cdot\boldsymbol{r}\boldsymbol{\alpha}^b\cdot\boldsymbol{r}}{r^3}\right). \quad (6)$$

This is the Coulomb potential divergent at $r \rightarrow 0$,

$$V_{\mathrm{conf}}(\boldsymbol{r}) = -\frac{\boldsymbol{\lambda}_a}{2}\frac{\boldsymbol{\lambda}_b}{2}\frac{3}{4}Kr, \quad (7)$$

which is a linear confinement potential divergent at $r \rightarrow \infty$,

$$V_{\mathrm{loop}}(\boldsymbol{r}) = \frac{\boldsymbol{\lambda}_a}{2}\frac{\boldsymbol{\lambda}_b}{2}\frac{6\pi}{25r}[v(\lambda r) - 1] - \frac{3\pi}{25}\Big[\frac{2v(\lambda r) + u(\lambda r) - 1}{r} + \frac{\partial u(\lambda r)}{\partial r}\Big]\boldsymbol{\alpha}^a \cdot\boldsymbol{\alpha}^b - \frac{3\pi}{25}\Big[-\frac{u(\lambda r)+1}{r^2} + \frac{1}{r}\frac{\partial u(\lambda r)}{\partial r} + \frac{\partial^2 u(\lambda r)}{\partial r^2}\Big]\frac{\boldsymbol{\alpha}^a\cdot\boldsymbol{r}\boldsymbol{\alpha}^b\cdot\boldsymbol{r}}{r}. \quad (8)$$

This is the potential originating from the loop corrections and being finite at any r. The functions $v(x)$ and $u(x)$ are defined as those in Ref. [14].

We decompose the wavefunctions into three parts,[15] orbital (Φ), colour (χ_c), and spin and flavour (χ_{sf}),

$$|\Psi\rangle = |\Phi\rangle \otimes |\chi_{sf}\rangle \otimes |\chi_c\rangle, \quad (9)$$

where $|\chi_c\rangle$ and $|\chi_{sf}\rangle$ of initial and final particles contribute to the colour factor and spin factor, respectively. The orbital wavefunctions for charmonia and mesons in the pseudoscalar octet and vector decuplet are obtained by solving the Schrödinger equation with the Buchmüller–Tye potential. The radial wavefunction of χ_{cJ} is parametrized as

$$R_{11}(\boldsymbol{r}) = 0.876\sqrt{Km_c}\rho(0.9e^{-0.5\rho^{1.6}} + 0.3e^{-6.4(\rho-0.2)}), \quad (10)$$

where $\rho = (Km_c)^{1/3}r$. The spatial wavefunction with quantum numbers is

$$\Phi_{11m}(\boldsymbol{r}) = R_{11}Y_{lm}\Big/\Big[\int_0^{\mathrm{d}'}\mathrm{d}rr^2R_{11}^2(r)\Big]^{1/2} \quad (11)$$

for $r \leq d'$ and zero for $r > d'$. Here d' is a monotonic function increasing with $r_{c\bar{c}}$, $d' = d'(r_{c\bar{c}})$, which is determined by

$$r_{c\bar{c}}^2 = \langle r\rangle^2 = \int\mathrm{d}^3r\,\Phi^*_{nlm}(\boldsymbol{r})r^2\,\Phi_{nlm}(\boldsymbol{r}). \quad (12)$$

The spatial wavefunctions of initial and final baryons are in a Gaussian form

$$\psi_N(\boldsymbol{r}_{12}, \boldsymbol{r}_{23}, \boldsymbol{r}_{31}) = \left(\frac{3a_1^2}{\pi^2}\right)^{3/4}\exp\left[\frac{a_1}{2}(r_{12}^2 + r_{23}^2 + r_{31}^2)\right] \quad (13)$$

for nucleons and

$$\psi_{c.b.}(\boldsymbol{r}_{12}, \boldsymbol{r}_{23}, \boldsymbol{r}_{31}) = \Big[\frac{m\pi^2}{m_c(2+\frac{m_c}{m})a_2{}^2}\Big]^{-3/4} \cdot\exp\Big[-\frac{a_2}{2}\Big(r_{12}^2 + \frac{m_c}{m}r_{23}^2 + \frac{m_c}{m}r_{31}^2\Big)\Big] \quad (14)$$

for charmed baryons. $m = 0.33\,\mathrm{GeV}$ and $m_c = 1.507\,\mathrm{GeV}$ are up (down) and charm quark masses respectively; $\boldsymbol{r}_{ij}$ is the relative coordinate of quarks i and j. In the wavefunctions, a_1 and a_2 are determined by fitting mass splittings between two baryons with spins 1/2 and 3/2 because of the spin–spin interaction. $a_1 = 1.388\,\mathrm{fm}^{-2}$ and $a_2 = 0.828\,\mathrm{fm}^{-2}$ give $m_\Delta - m_N = 0.298\,\mathrm{GeV}$ and $m_{\Sigma_c} - m_{\Lambda_c^+} = 0.162\,\mathrm{GeV}$ compared to the experimental values 0.293 GeV and 0.168 GeV, respectively. The results for mass splittings show that the wavefunctions are reliable.[10] The Fourier transform of the two wavefunctions produces $\psi_N(\boldsymbol{p}_{12}, \boldsymbol{p}_{23}, \boldsymbol{p}_{31})$ and $\psi_{c.b.}(\boldsymbol{p}_{12}, \boldsymbol{p}_{23}, \boldsymbol{p}_{31})$ for the relative momentum p_{ij} of two quarks, which are used to calculate the baryon–charmonium scattering cross sections.

We calculate $\langle \Psi_{q_1q_2q_3} | \langle \Psi_{c\bar{c}} | (V_{\rm coul} + V_{\rm conf} + V_{\rm loop}) | \Psi_{\bar{c}'q_3'} \rangle | \Psi_{q_1'q_2'c'} \rangle$ but label final quarks and anti-quarks with primes to show different momenta due to the virtual gluon interaction. The quark (anti-quark) momentum is denoted by $\boldsymbol{p}_i$ ($i = q_1, q_2, q_3, c, \bar{c}, q_1', q_2', q_3', c', \bar{c}'$). Conservation of momenta allows that only three quark (or anti-quark) momenta are independent. All the relative momenta of quarks and anti-quarks in mesons can be expressed in terms of the independent variables. Integrals with the independent variables yield

$$
\begin{aligned}
\mathcal{M}_{q_1\bar{c}} =& \langle \Psi_{q_1q_2q_3} | \langle \Psi_{c\bar{c}} | V_{q_1\bar{c}}(\boldsymbol{p}_{q_1'} - \boldsymbol{p}_{q_1}) | \Psi_{q_1'q_2'c'} \rangle | \Psi_{q_3'\bar{c}'} \rangle \\
=& \int \frac{\mathrm{d}^3\boldsymbol{p}_{q_1}}{(2\pi)^3} \int \frac{\mathrm{d}^3\boldsymbol{p}_{q_2}}{(2\pi)^3} \int \frac{\mathrm{d}^3\boldsymbol{p}'_{q_1}}{(2\pi)^3} \\
& \cdot \Psi^\dagger_{q_1q_2q_3} \Psi_{c\bar{c}}{}^\dagger V_{q_1\bar{c}}(\boldsymbol{p}_{q_1'} - \boldsymbol{p}_{q_1}) \Psi_{q_1'q_2'c'} \Psi_{q_3'\bar{c}'},
\end{aligned} \tag{15}
$$

where $\boldsymbol{p}_{q_1q_2} = \frac{\boldsymbol{p}_{q_1} - \boldsymbol{p}_{q_2}}{2}$, $\boldsymbol{p}_{q_2q_3} = \frac{\boldsymbol{p}_{q_1} - \boldsymbol{p}_{cm}}{2} + \boldsymbol{p}_{q_2}$, $\boldsymbol{p}_{q_3q_1} = \frac{\boldsymbol{p}_{cm} - \boldsymbol{p}_{q_2}}{2} - \boldsymbol{p}_{q_1}$; $\boldsymbol{p}_{c\bar{c}} = \frac{\boldsymbol{p}_{cm}}{2} + \boldsymbol{p}'_{cm} - \boldsymbol{p}_{q_1'} - \boldsymbol{p}_{q_2}$; $\boldsymbol{p}_{q_1'q_2'} = \frac{\boldsymbol{p}_{q_1'} - \boldsymbol{p}_{q_2}}{2}$, $\boldsymbol{p}_{q_2'c'} = \frac{m}{m+m_c}(\boldsymbol{p}_{q_1'} - \boldsymbol{p}'_{cm}) + \boldsymbol{p}_{q_2}$, $\boldsymbol{p}_{c'q_1'} = \frac{m}{m+m_c}(\boldsymbol{p}'_{cm} - \boldsymbol{p}_{q_2}) - \boldsymbol{p}_{q_1'}$; $\boldsymbol{p}_{q_3'\bar{c}'} = \frac{m}{m+m_c}\boldsymbol{p}'_{cm} + \boldsymbol{p}_{cm} - \boldsymbol{p}_{q_1} - \boldsymbol{p}_{q_2}$. $\mathcal{M}_{q_2\bar{c}}$, $\mathcal{M}_{q_3\bar{c}}$, $\mathcal{M}_{q_1c}$, $\mathcal{M}_{q_2c}$ and $\mathcal{M}_{q_3c}$ can be obtained in the same way as $\mathcal{M}_{q_1\bar{c}}$.

We need calculate $\langle \boldsymbol{s}_a \cdot \boldsymbol{s}_b \rangle$ for the spin–spin interactions and the overlap of initial and final wavefunctions for the spin-independent potential. Since these spin matrix elements involve total spin of initial and final states, the reactions $A + B \to C + D$ comprising nine channels are:

(1) $p + \chi_{cJ} \to \Lambda_c^+ + \bar{D}^0$,
(2) $p + \chi_{cJ} \to \Lambda_c^+ + \bar{D}^{*0}$ $(s = 1/2)$,
(3) $p + \chi_{cJ} \to \Lambda_c^+ + \bar{D}^{*0}$ $(s = 3/2)$,
(4) $p + \chi_{cJ} \to \Sigma_c^{++} + D^-$,
(5) $p + \chi_{cJ} \to \Sigma_c^{++} + D^{*-}$ $(s = 1/2)$,
(6) $p + \chi_{cJ} \to \Sigma_c^{++} + D^{*-}$ $(s = 3/2)$,
(7) $p + \chi_{cJ} \to \Sigma_c^{*++} + D^-$,
(8) $p + \chi_{cJ} \to \Sigma_c^{*++} + D^{*-}$ $(s = 1/2)$,
(9) $p + \chi_{cJ} \to \Sigma_c^{*++} + D^{*-}$ $(s = 3/2)$.

The matrix element in Eq. (15) indicates that the squared amplitude $|\mathcal{M}|^2$ in Eqs. (1) and (3) are the functions of $\boldsymbol{p}_{cm}$ and $\boldsymbol{p}'_{cm}$. Charmonium dissociation cross sections versus $\sqrt{s}$ the centre-of-mass energy of the charmonium and baryon in the above nine channels are plotted in Figs. 1–3.

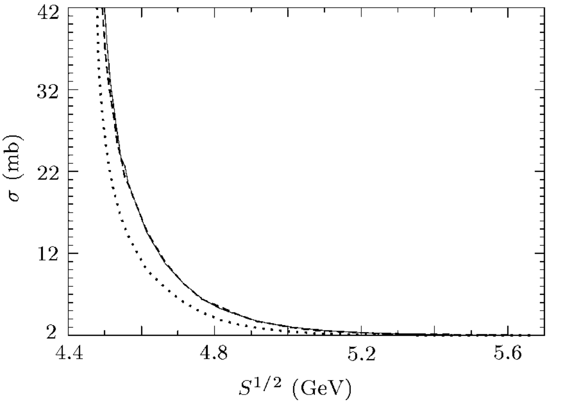

Fig. 1. Cross sections for $p+\chi_{c1} \to \Lambda_c^+ \bar{D}^0$ (solid), $\Lambda_c^+ \bar{D}^{*0}$ $(s = 1/2)$ (dotted) and $\Lambda_c^+ \bar{D}^{*0}$ $(s = 3/2)$ (dashed).

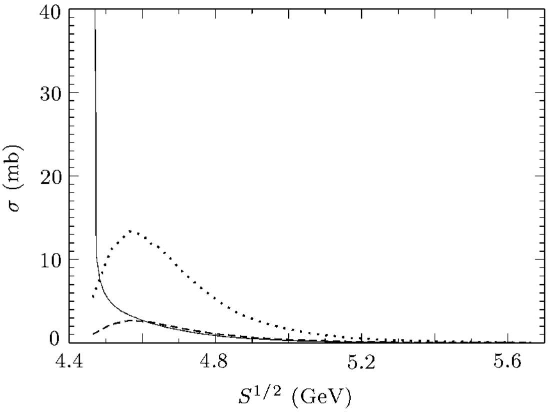

Fig. 2. Cross sections for $p + \chi_{c1} \to \Sigma_c^{++} D^-$ (solid), $\Sigma_c^{++} D^{*-}(s = 1/2)$ (dotted), $\Sigma_c^{++} D^{*-}(s = 3/2)$ (dashed).

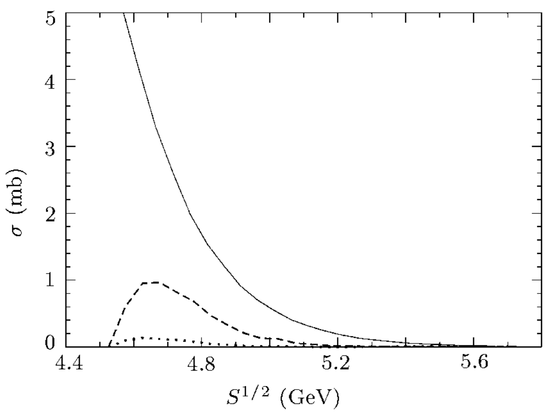

Fig. 3. Cross sections for $p + \chi_{c1} \to \Sigma_c^{*++} D^-$ (solid), $\Sigma_c^{*++} D^{*-}(s = 1/2)$ (dotted), $\Sigma_c^{*++} D^{*-}(s = 3/2)$ (dashed).

All the reactions are divided into two types: endothermic and exothermic reactions. The relative momentum of outgoing particles and the cross section are zero at the threshold energy $s_0 = (m_1 + m_2)^2$ for an endothermic reaction, while the relative momentum of incoming particles is zero and the cross section is infinite at the threshold energy $s_0 = (m_3 + m_4)^2$ for an exothermic reaction. We find that the momentum ratio P'_{cm}/P_{cm} increases very rapidly from the threshold energy to the centre-of-mass energy at the peak for each line in the figures, but slowly further and approaches 1. Then the matrix element

$$\mathcal{M} = \mathcal{N}\langle \Psi_{q_1q_2q_3}|\langle \Psi_{c\bar{c}}|(V_{q_1\bar{c}} + V_{q_2\bar{c}} + V_{q_3\bar{c}} + V_{q_1c} + V_{q_2c} + V_{q_3c})|\Psi_{q_1q_2c}\rangle|\Psi_{q_3\bar{c}}\rangle$$

controls the dependence of cross section on the centre-of-mass energy $\sqrt{s}$ and makes the cross section decline. Our results agree with the dissociation cross section induced by mesons of Ref. [12].

Furthermore, the cross sections are very important for the dissociation of χ_{cJ} in hadronic matter since final hadron momentum offers relatively low centre-of-mass energy. The dissociation cross sections of χ_{cJ} have direct relation with prompt J/Ψ measured by experiments. The accuracy of our new cross sections are examined by the χ_{cJ} suppression in the $p-A$ collisions, which is being measured by the HERA-B collaboration. Furthermore, RHIC and ALICE experiments in the future will also examine our results.

We gratefully acknowledge Professor X. Cai and Professor T. C. Meng for useful discussions.

References

[1] Kharzeev D *Preprint* nucl-th/9802037

[2] Kharzeev D 1996 *Nucl. Phys.* A **610** 418c
Wong C Y 1996 *Nucl. Phys.* A **610** 434c
Wong C Y 1997 *Phys. Rev.* C **55** 2621
Wong C Y *Preprint* hep-ph/9712332

[3] Xu X M 1999 *Nucl. Phys.* A **658** 165

[4] Braun-Munzinger E P et al 1996 *Nucl. Phys.* A **610** 404c

[5] Ramello L, Gonin M, Braun-Munzinger E P et al 1996 *Nucl. Phys.* A **610** 404c.

[6] HERA-B *Report on Status and Progress Preprint* DESY-PRC 00/04

[7] Biro T S, VanDoorn E, Müller B, Thoma M H and Wang X N 1993 *Phys. Rev.* C **48** 1275

[8] Levai P, Müller B and Wang X N 1995 *Phys. Rev.* C **51** 3326

[9] Bodwin G T, Braaten E and Lepage G P 1995 *Phys. Rev.* D **51** 1125

[10] Xu X M 2002 *Nucl. Phys.* A **697** 825

[11] Matinya S G, Matinyan G and Muller B 1998 *Phys. Rev.* C **58** 2994

[12] Martins K, Blasche D and Quack E 1995 *Phys. Rev.* C **51** 2723

[13] Buchmüller W and Tye S H H 1981 *Phys. Rev.* D **24** 132

[14] Matsui T and Satz H 1986 *Phys. Lett.* B **178** 416

[15] Barnes T 1992 *Phys. Rev.* D **46** 131
Swanson E S 1992 *Ann. Phys.* **220** 73